Penerbit Akademia Baru

Journal of Advanced Research in Fluid Mechanics and Thermal Sciences

Journal homepage: www.akademiabaru.com/arfmts.html
ISSN: 2289-7879

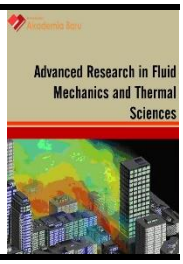

Simulation of Oldroyd-B Viscoelastic Fluid in Axisymmetric Straight Channel by Using a Hybrid Finite Element/Volume Method

Ihssan Aqeel Fadhel[1], Alaa Hassan Al-Muslimawi[2,*]

[1] Department of Mathematics, College of Education for Pure Sciences, University of Basrah, Basrah, Iraq
[2] Department of Mathematics, College of Sciences, University of Basrah, Basrah, Iraq

ARTICLE INFO

Article history:
Received 16 September 2020
Received in revised form 30 November 2020
Accepted 1 December 2020
Available online 11 March 2021

Keywords:
Axisymmetric straight channel; Galerkin method; Hybrid finite element/volume; Oldroyd-B model; Viscoelasticity

ABSTRACT

In this study, incompressible viscoelastic fluid through the axisymmetric circular channel is simulated with Oldroyd-B model. The simulation is performed based on a hybrid finite volume/element method, which consists of Taylor-Galerkin finite element discretisation, and a cell vertex fluctuation-distribution finite volume method. In this context, the momentum and continuity equations are treated with a finite element method, while a finite volume approach is applied to solve the Oldroyd-B constitutive model. Analytical expressions are presented for the velocity and stress components in fully developed channel flow of Oldroyd-B fluid. For this complex fluid, we see an excellent agreement between the analytic and the numerical solutions. The study of axisymmetric circular channel problem based on a hybrid numerical method represents a great challenge. The novelty here is to study the temporal convergence-rate of the system solution that is taken to be steady state, incompressible, axisymmetric, and laminar, which did not address by researchers previously. Here, the rate of convergence for all solution components is presented, where a large level of convergence is appeared for stress compared to the other solution components. Moreover, the pressure drops and stress response across the flow are provided with respect to difference in solvent-fraction (β) and Weissenberg number (We). A significant effect from the viscoelastic parameters upon the level of the stress has been detected, while for the pressure response the change is semi-modest. For the stress response the findings reveal that, with decreasing solvent-fraction (β), the maxima level of stress components are strongly amplifies.

1. Introduction

In this study of the complex axisymmetric flow through a channel using the constitutive equation representation of the Oldroyd-B model is investigated. Numerically, the hybrid finite element/finite volume (fe/fv) method represents one of the best algorithms to treat such problems [1]. The main idea of such method is to combine the finite element method with a cell-vertex finite volume approach to solve the viscoelastic governing equations. Consequently, the Galerkin finite element method has been implemented to treat the mass conservation and momentum transport equations

* *Corresponding author.*
E-mail address: alaa.abdullah@uobasrah.edu.iq

https://doi.org/10.37934/arfmts.81.1.2640

due to that this implementation is best for self-related problems, and therefore are perfect for discretization of elliptic operators. Furthermore, finite volume technique has progressed a lot over the past decade in its treatment of the first-order hyperbolic equations, and therefore it has been selected to solve stress constitutive model [2].

There is extensive literature on methods of finite elements for viscoelastic flows. Recently, a few powerful methods have shown that it is possible to treat some complicated problems such as highly elastic and non-smooth flows [3,4]. Due to that, the finite element approach does not carry with a strong computational of complex flow problems that require developed numerical techniques in dealing with velocity gradients accuracy, supper stability, coupling of the system, and up winding. Thus, this point represents an important problem that must be addressed, especially for three dimensional, and multi-mode viscoelastic [5-8]. For this reason several attempts have been made to propose alternative strategies to overcome the difficulties that were encountered. One alternative in this respect is applying the fv approach, which derives from the finite difference scheme and needs less memory and CPU time compared to fe scheme [9]. This method is perfect for hyperbolic systems, where the source terms are given as associated area integrals, with incorporating the fluxes of the system as integrals on boundaries of control volumes. The study of viscoelastic problems by using fv methods fall into two classes; a pure fv form and a hybrid (fe/fv) implementation. Hybrid methods were proposed by Sato and Richardson [10] and Yoo and Na [11]. There, the hybrid (fe/fv) method is achieved fv for pressure and stress and a fe approach for momentum. Wapperom and Webster [1] also proposed the hybrid (fe/fv) scheme as alternative strategy for the one used by Sato and Richardson [10]. In this implementation the finite element discretisation is used for momentum and continuity equations and finite volume method for stress constitutive equation. In addition, Wapperom and Webster [12] studied the stability of this method on the basis of flows as the Weissenberg number increased. Moreover, Aboubacar and Webster [13] and Aboubacar *et al.,* [14] have shown that a specific of a cell-vertex hybrid finite volume/element method is suitable for calculating highly elastic solutions of Oldroyd-B and Phan-Thien/ Tanner (PTT) in plane $4:1$ contraction flows for Cartesian coordinates.

A hybrid (fe/fv) method has been widely implemented to examine viscoelastic problems, where it is shown to have high advantage [15-18]. Furthermore, (fe/fv) is utilized for free surface viscoelastic problems. In this context, Al-Muslimawi *et al.,* [19,20] and Al-Muslimawi [21] implemented the (fe/fv) for annular axisymmetric tube-tooling cable-coating.

Furthermore, the study of viscoelastic complex axisymmetric flow through a channel represents one of the important issues in the rheology field. For that, many real applications to such problem with the considered effects have been presented in the various studies. For example, in the industrial field, recently there are numerical and theoretical interest in investigating the role of Newtonian and non-Newtonian characteristics on the structure of the flow field in conduits [22,23]. Moreover, the literature on nanofluids is broad. In that field many studies of recent years have conducted [24-26].

In the present study, the a hybrid finite element/finite volume discretisation (fe/fv) has been used for the treatment of complex axisymmetric flow through a channel. The Oldroyd-B model is used to discuss such specific problem. A numerical technique is used for triangular fe meshes with fv sub-cells. In this context, the first velocity and stress components are expected to a half time-step, then updated over the full time-step. To ensure the incompressibility restrictions, the pressure in the forward time step is derived from the Poisson equation, with velocity correction in the final stage to satisfy continuity. The novelty here is to study the temporal convergence-rate of the system solution that is taken to be steady state, incompressible, axisymmetric, and laminar, which did not address by researchers previously. In this context, Oldroyd-B viscoelastic fluid along a two-dimensional axisymmetric straight channel, under isothermal condition is studied. The main results of current

study focused on the convergence rate of velocity, pressure and stress solutions under the variation solvent-fraction (β). Furthermore, The effect of the Weissenberg number and solvent-fraction on the behaviours of solution has also been investigated.

2. Governing Equations

The system of dimensionless governing equations that consists of the continuity equation and momentum equation can be expressed as follows

$$\nabla \cdot u = 0, \tag{1}$$

$$Re\frac{\partial u}{\partial t} = \nabla \cdot T - Re(u \cdot \nabla u) - \nabla p, \tag{2}$$

where, u, p and Re are the velocity, pressure of fluid and Reynolds number, respectively, and ∇ denotes the gradient operator, and T represents the extra stress tensor, which is given by

$$T = 2\mu_s d + \tau.$$

Correspondingly, the rate of deformation d for general flows is expressed as

$$d = \frac{1}{2}(\nabla u + \nabla u^{\dagger}),$$

and

$$\tau + \lambda_1 \overset{\nabla}{\tau} = 2\mu_p d. \tag{3}$$

Where μ_s , μ_p and λ_1 are polymeric viscosity, solvent viscosity contributions and relaxation time of fluid, respectively, and † is tensor transpose. In addition, ($\overset{\nabla}{\tau}$) represents the upper convected stress derivative, which is defined as

$$\overset{\nabla}{\tau} = \frac{\partial \tau}{\partial t} + u \cdot \nabla \tau - \nabla u^{\dagger} \cdot \tau - \tau \cdot \nabla u. \tag{4}$$

From Eq. (3) and Eq. (4), the Oldroyd-B constitutive model can be gathered as

$$\lambda_1 \frac{\partial \tau}{\partial t} = \left(2\mu_p d - \tau\right) - \lambda_1(u \cdot \nabla \tau - \nabla u^{\dagger} \cdot \tau - \tau \cdot \nabla u). \tag{5}$$

The non-dimensional structure of the Oldroyd-B constitutive model in Eq. (5) can be formed via velocity scale U, length scale L (unit length), time scale L/U, and pressure and extra-stress scale of $\mu U/L$. The parameter $\mu = \mu_s + \mu_p$ is the total viscosity, consisting of consistent viscosity fractions for solvent and solute. Here, the dimensional parameters are presented in the form of Weissenberg number We and solvent β, which are presented by

$$We = \lambda_1 \frac{U}{L}, \beta = \frac{\mu_s}{\mu_s + \mu_p} = \frac{\mu_s}{\mu}. \tag{6}$$

Therefore, the dimensionless form of the Oldroyd-B constitutive model with an important parameter We is given by

$$We\frac{\partial \tau}{\partial t} = 2(1-\beta)d - \tau - We(u\cdot\nabla\tau) + We(\nabla u^{\dagger}\cdot\tau + \tau\cdot\nabla u). \quad (7)$$

3. Numerical Method

3.1 Taylor Galerkin-pressure Correction Discretisation

In this study the basis of the numerical procedure to treat the system of current differential equations is a $TS-TG-PC-FEM$, which is proposed by Townsend and Webster [27]. The general framework of this method involves two essential aspects: a Taylor-Galerkin scheme and a pressure-correction scheme. The Taylor-Galerkin scheme is a two-step Lax-Wendroff time stepping procedure, extracted via a Taylor series expansion in time [28,29]. The pressure-correction method accommodates the incompressibility constraint to ensure second-order accuracy in time by adopting a semi-implicit Crank-Nicolson time-split with time increment factor θ_{cr} [14]. Three fractional-staged formulations with non-dimensional parameters within each time-step may be given by

$$Stage\ 1a: \frac{2Re}{\Delta t}\left[u^{n+\frac{1}{2}} - u^{n}\right] = [\nabla\cdot(\tau + 2\beta d) - Reu\cdot\nabla u - \nabla p]^{n}, \quad (8)$$

$$\frac{2We}{\Delta t}\left[\tau^{n+\frac{1}{2}} - \tau^{n}\right] = [2(1-\beta)d - \tau + We(\nabla u\cdot\tau + \tau\cdot(\nabla u)^{\dagger})]^{n}, \quad (9)$$

$$Stage\ 1b: \frac{Re}{\Delta t}[u^{*} - u^{n}] = [\nabla\cdot(\tau + 2\beta d) - Reu\cdot\nabla u]^{n+\frac{1}{2}} - \nabla p^{n}, \quad (10)$$

$$\frac{We}{\Delta t}[\tau^{n+1} - \tau^{n}] = [2(1-\beta)d - \tau + We(\nabla u\cdot\tau + \tau\cdot(\nabla u)^{\dagger})]^{n+\frac{1}{2}}, \quad (11)$$

$$Stage\ 2: \nabla^{2}(p^{n+1} - p^{n}) = \frac{Re}{\theta_{cr}\Delta t}\nabla\cdot u^{*}, \quad (12)$$

$$Stage\ 3: u^{n+1} = u^{*} - \frac{\theta_{cr}\Delta t}{Re}[\nabla(p^{n+1} - p^{n})]. \quad (13)$$

In these fractional stages the velocity and stress fields are calculated at the half time-step $(u,\tau)^{n+\frac{1}{2}}$ and corrected for the full time-step $(u^{*},\tau)^{n+1}$ ($Stage\ 1$). To improve the convergence and stability of the solution, the momentum diffusion term is treated in a semi-implicit way. The velocity field (u^{*}), which is derived through the full time-step of the momentum, may not satisfy continuity and require a correction. Thus, a Poisson-like equation is generated to increase the time step of pressure ($Stage\ 2$), accompanied with a correction ($Stage\ 3$).

3.2 Sub-vertex Finite Volume Discretisation

To outline the application of the fv-theory, we rewrite the Oldroyd-B stress constitutive (Eq. (7)) into conservative form, and identify the flux (R) and source (Q) terms, viz [30].

$$\frac{\partial \tau}{\partial t} = -R + Q, \quad (14)$$

$$R = u\tau, \tag{15}$$

$$Q = \frac{1}{We}(2(1-\beta)d - \tau) + \nabla u^{\dagger} \cdot \tau + \tau \cdot \nabla u. \tag{16}$$

Then, cell-vertex fv-approaches are implemented to this constitutive equation using fluctuation distribution as the upwinding strategy, to distribute control volume residuals and furnish nodal solution updates [1]. Consider each scalar stress component, τ, acting on an arbitrary volume $\Omega = \sum_l \Omega_l$, whose variation is controlled through corresponding fluctuation components of flux (R) and source (Q),

$$\frac{\partial}{\partial t}\int_{\Omega_l} \tau d\Omega = -\int_{\Omega_l} R d\Omega + \int_{\Omega_l} Q d\Omega. \tag{17}$$

The integral source variations and flux have been calculated over each finite volume triangle (Ω_l), and are appropriated proportionally by the chosen cell-vertex distribution method to its three vertices. The update of nodal is gained, by summing all contributions from its control volume Ω_l, composed of all fv-triangles surrounding node (l) (see Figure 1(b)). Moreover, the flux and source residuals probably determined through two separate control volumes associated with a given node (l) within the fv-cell T, generating two contributions, one upwinded and governed over the fv-triangle T, (R_T, Q_T), and a second area-averaged and subtended over the median-dual-cell zone, (R_{MDC}, Q_{MDC}). For reasons of temporal accuracy, this procedure demands appropriate area-weighting to maintain consistency, with extension to time-terms likewise. In this context, a generalized fv-nodal update equation is derived per stress component, by separate treatment of individual time derivative, flux and source terms, and integrating over associated control volumes, given,

$$\left[\sum_{\forall T_l} \delta_T \alpha_l^T \Omega_T + \sum_{\forall MDC_l} (1-\delta_T)\widehat{\Omega}_l^T\right]\frac{\Delta\tau_l^{n+1}}{\Delta t} = \sum_{\forall T_l} \delta_T \alpha_l^T b^T + \sum_{\forall MDC_l} (1-\delta_T) b_l^{MDC}, \tag{18}$$

where $b^T = (-R_T + Q_T)$, $b_l^{MDC} = (-R_{MDC} + Q_{MDC})^l$, Ω_T is the area of the fv-triangle T, and (10×20) elements is the area of its median-dual-cell (MDC). The weighting parameter, $0 \leq \delta_T \leq 1$, proportions the balance taken between the contributions from the median-dual-cell and the fv-triangle T. The discrete stencil (18) identifies fluctuation distribution and median dual cell contributions, area weighting and upwinding factors (α_l^T-scheme dependent) [1].

3.3 The Low Difiusion B (LDB) Scheme

Al-Muslimawi *et al.,* [19] and Aboubacar *et al.,* [31] have shown that the Low Diffusion B (LDB) approach is a suitable choice to determine the fluctuation distribution parameter α. This is a linear method with the properties of linearly preservation and accuracy of the second order [31]. The LDB distribution coefficients α_i are determined on each triangle via angles γ_1, γ_2 see Figure 2, subtended at an inflow vertex (i) by the advection velocity a, where a is average of velocity field per fv-cell, viz

$$\alpha_i = \frac{\sin\gamma_1 \cos\gamma_2}{\sin(\gamma_1+\gamma_2)}, \alpha_j = \frac{\sin\gamma_2 \cos\gamma_1}{\sin(\gamma_1+\gamma_2)}, \alpha_k = 0. \tag{19}$$

Note that, if $\gamma_1 > \gamma_2$, then $\alpha_i > \alpha_j$, and thus, by design, node (i) has a greater contribution than flow from node (j).

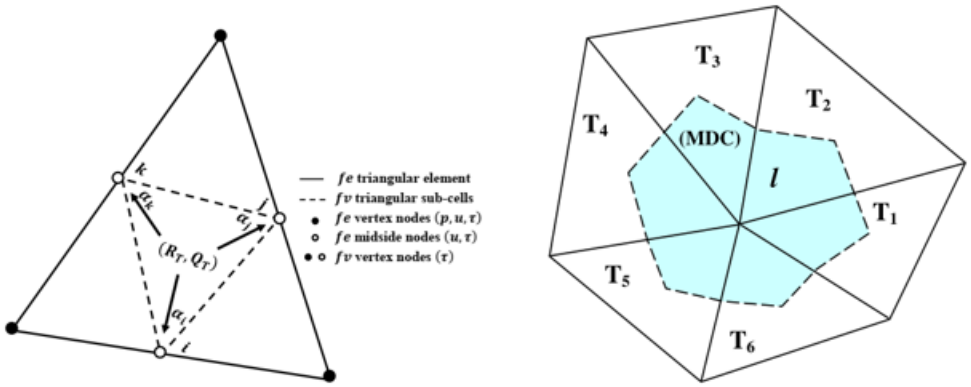

Fig. 1. Schematic diagram, fe/fv discretisation

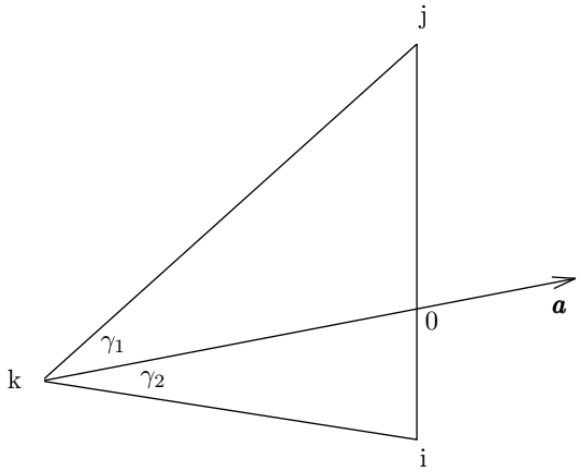

Fig. 2. LDB-scheme, defining γ_1 and γ_2 in fv cell

4. Problem Specification and Boundary Conditions

Poiseuille flow through a two dimensional axisymmetric straight channel is introduced in this study under isothermal condition. The symmetry is taken around the central flow line, which allows searching for solutions on the upper, where the radial velocity at the centerline has vanished. Consequently, we handle motion in a plane layer, say $\{(x, y) \in R^2\} \times \{z \in (0, h)\}$. For this purpose, a triangular finite element is implemented.

4.1 Boundary Conditions (BCs)

The setting of BC_s of the present channel problem is laid as follows

i. The inflow conditions are chosen to be those corresponding to the analytical expressions for fully-developed axial velocity, such that $u_z = u_{max}(1 - r^2)$.
ii. No-slip BCs is applied on the top and bottom walls of the channels.
iii. Zero radial velocity applies and zero pressure are applied on the outlet of the channels.

5. Numerical Results

The numerical results are computed for Viscoelastic flow through axisymmetric straight channel by taking a circular cross section of pipe. The results are shown for $h = 1$, Crank-Nicolson parameter $\theta = 0.5$, tolerance criteria taken here as 10^{-6} and typical Δt is $O(10^{-4})$.

5.1 Analytic Solution

For fully developed shear axisymmetric fluids through a circular channel, the solution in axial velocity can be computed analytically under specific conditions. In the case of the axisymmetric flow with vanish tangential and radial velocities $(u_r = u_\theta = 0)$, $\frac{\partial p}{\partial r} = 0, \frac{\partial p}{\partial \theta} = 0$ and $\frac{\partial p}{\partial z}$ is constant. Thus, under these assumptions the dimensional velocity solution [32]

$$u_z = (u_z)_{max}\left(1 - \frac{r^2}{R^2}\right), \tag{20}$$

where, R is the radial of the channel and $(u_z)_{max}$ is the maximum velocity in the fully developed flow region.

$$(u_z)_{max} = \frac{R^2 \Delta p}{4\beta l}, \tag{21}$$

such that, $\Delta p = p_2 - p_1$, where p_1 and p_2 are the pressures at the outlet and inlet of the pipe, respectively, and l is its length.

In addition, for Oldroyd-B model the analytic solution for the shear stress τ_{rz} and normal stress τ_{zz} can be computed as

The Eq. (7) can be written as

$$\tau_{rr} + We\left[u_r \frac{\partial \tau_{rr}}{\partial r} + u_z \frac{\partial \tau_{rr}}{\partial z} - 2\left(\tau_{rr}\frac{\partial u_r}{\partial r} + \tau_{rz}\frac{\partial u_r}{\partial z}\right)\right] = 2(1-\beta)\frac{\partial u_r}{\partial r} \tag{22}$$

$$\tau_{rz} + We\left[u_r \frac{\partial \tau_{rz}}{\partial r} + u_z \frac{\partial \tau_{rz}}{\partial z} - \left(\tau_{rr}\frac{\partial u_z}{\partial r} + \tau_{rz}\left(\frac{\partial u_z}{\partial z} + \frac{\partial u_r}{\partial r}\right) + \tau_{zz}\frac{\partial u_r}{\partial z}\right)\right] = (1-\beta)\left(\frac{\partial u_r}{\partial z} + \frac{\partial u_z}{\partial r}\right) \tag{23}$$

$$\tau_{zz} + We\left[u_r \frac{\partial \tau_{zz}}{\partial r} + u_z \frac{\partial \tau_{zz}}{\partial z} - 2\left(\tau_{rz}\frac{\partial u_z}{\partial r} + \tau_{zz}\frac{\partial u_z}{\partial z}\right)\right] = 2(1-\beta)\frac{\partial u_z}{\partial z} \tag{24}$$

Under the assumptions

$$u_r = 0, \frac{\partial \tau_{rz}}{\partial z} = 0, \qquad \tau_{rr} = 0, \qquad \frac{\partial u_z}{\partial z} = \frac{\partial u_r}{\partial r} = \frac{\partial u_r}{\partial z} = 0$$

These equations are reduced to

$$\begin{aligned} &\tau_{rz} = (1-\beta)\frac{\partial u_z}{\partial r}, but\ u_z = (u_z)_{max}\left(1 - \frac{r^2}{R^2}\right) \\ &\tau_{rz} = (1-\beta)\left(\frac{-2r}{R^2}(u_z)_{max}\right) = -\frac{2r(1-\beta)}{R^2}(u_z)_{max} \end{aligned} \tag{25}$$

From Eq. (24) we have

$$\tau_{zz} + We\left[0 + 0 - 2\left(\tau_{rz}\frac{\partial u_z}{\partial r} + 0\right)\right] = 0 \rightarrow \tau_{zz} = 2We\,\tau_{rz}\frac{\partial u_z}{\partial r}$$

From Eq. (25) and $u_z = (u_z)_{max}\left(1 - \frac{r^2}{R^2}\right)$ we have

$$\tau_{zz} = 2We\left(-\frac{2r(1-\beta)}{R^2}(u_z)_{max}\right)\left(\frac{-2r}{R^2}(u_z)_{max}\right)$$
$$\tau_{zz} = 8We\,(1-\beta)\frac{r^2}{R^4}((u_z)_{max})^2 \quad (26)$$

Comparison between the numerical results and analytic solution for fully developed velocity, stress components is considered. The profile of analytical and numerical axial velocities in the fully developed flow is shown in Figure 3(a). Here, the numerical results are provided under the imposition of the axial velocity corresponding to the analytical expressions of the full evolution (19), with $(u_z)_{max}$ set to unity, *We*=3 and β=0.9. The findings demonstrate that the numerical results give full agreement with the available analytical solutions. Again, for same setting of parameters, Figure 3(b) and Figure 3(c) show the numerical solutions for the shear stress (τ_{rz}), normal stress (τ_{zz}) versus the analytical solution. It can be seen that the agreement between numerical and analytical solutions is good, which adequately reflects the power of our numerical technique.

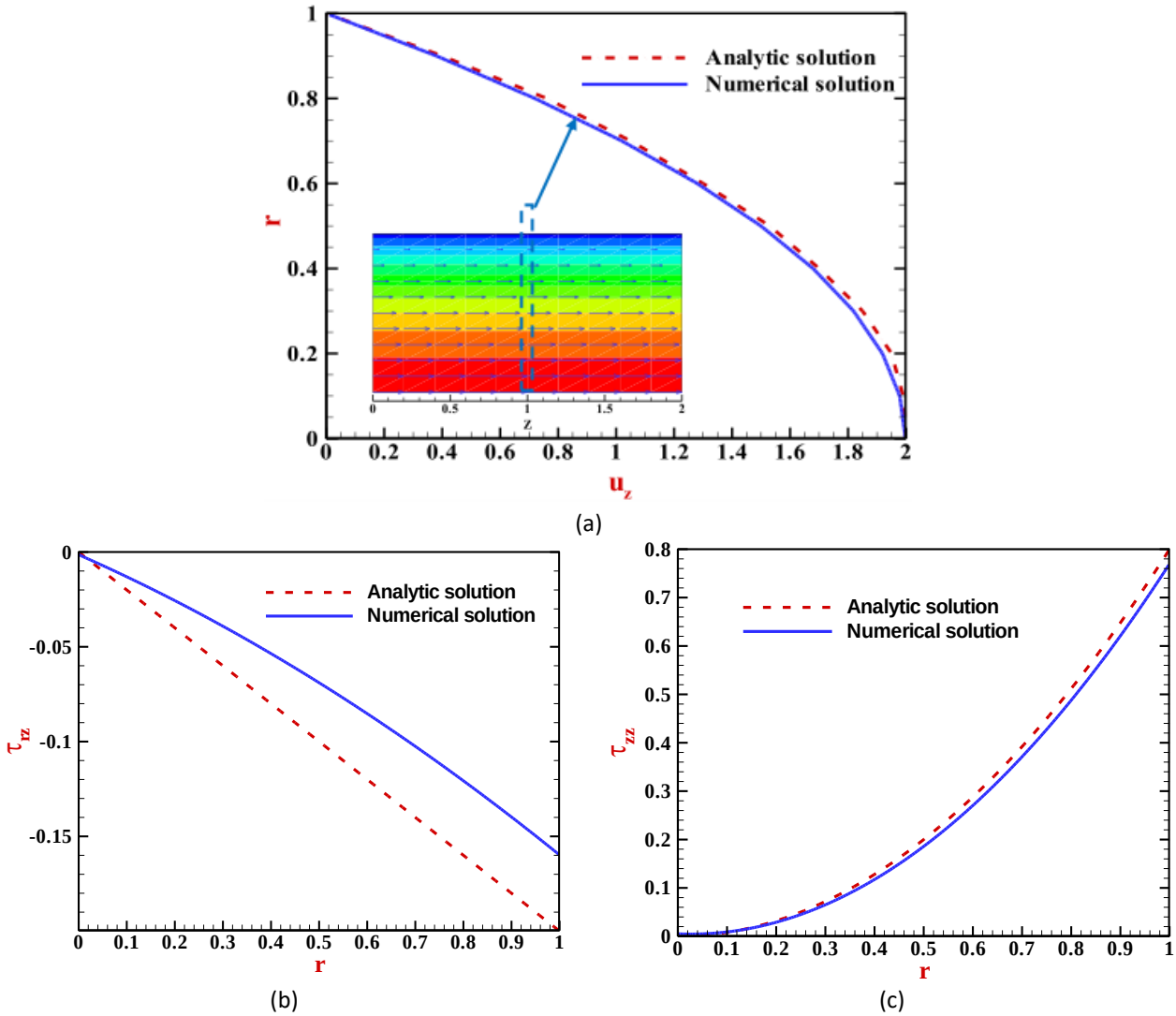

Fig. 3. Comparison between the analytic and numerical (*We*=3 and β=0.9) solutions (a) axial velocity, (b) shear stress, (c) normal stress

History plots of the relative error increment norms in velocity, pressure and stress are illustrated in Figure 4 for $We = 1$ and $\beta = 0.9$. The findings reflect a lower rate of convergence for the velocity compared to that extracted for pressure and stress under the same rate of time-stepping convergence.

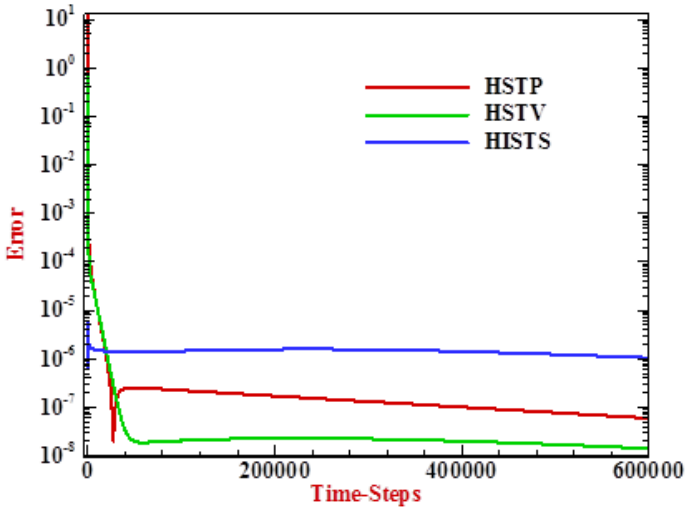

Fig. 4. Rate of convergence; $We = 1, \beta = 0.9$

In addition, the error of solution for velocity, pressure and stress components is provided in Table 1 for the different values of We and $\beta = 0.9$. Generally, the level of stress error is slightly higher than that relevant to velocity and pressure components, which reflects the difficulties of stress calculation for the viscoelastic Oldroyd-B fluid.

Table 1
Comparison of error and time ; We-various, $\beta = 0.9$

		Time				
We-various	Error	0.2	0.8	2	5	6
1	$\|u_z\|_{L_2}$	7.1×10^{-3}	1.9×10^{-6}	6.2×10^{-6}	1.7×10^{-6}	1.4×10^{-7}
	$\|p\|_{L_2}$	1.3×10^{-4}	2.1×10^{-5}	1.1×10^{-5}	7.1×10^{-6}	5.1×10^{-7}
	$\|\tau\|_{L_2}$	1.8×10^{-4}	1.6×10^{-4}	1.5×10^{-4}	1.2×10^{-4}	1.1×10^{-5}
2	$\|u_z\|_{L_2}$	1.3×10^{-4}	3.3×10^{-6}	2.3×10^{-6}	2.1×10^{-6}	1.8×10^{-7}
	$\|p\|_{L_2}$	1.1×10^{-4}	2.1×10^{-5}	1.5×10^{-5}	6.5×10^{-6}	4.7×10^{-7}
	$\|\tau\|_{L_2}$	2.2×10^{-4}	1.8×10^{-4}	1.5×10^{-4}	1.1×10^{-4}	1.3×10^{-5}
3	$\|u_z\|_{L_2}$	1.3×10^{-4}	3.4×10^{-6}	3.2×10^{-6}	2.6×10^{-6}	2×10^{-7}
	$\|p\|_{L_2}$	1.1×10^{-4}	2.8×10^{-5}	1.8×10^{-5}	6.7×10^{-6}	4.9×10^{-7}
	$\|\tau\|_{L_2}$	2.4×10^{-4}	1.9×10^{-4}	1.6×10^{-4}	1.7×10^{-4}	1.4×10^{-5}

In Figure 5(a), the pressure drop of the fluid for $\beta = 0.9$ and three different We-values ($We = \{1,2,3\}$) is presented. The results reveal that, there is a variation in the level of pressure at the channel inlet, where for Newtonian solutions an overall maximum of 8 units is observed, while for viscoelastic Oldroyd-B model this level is slightly reduced to be around 7.5 units where is attributed to shear-thinning effects. Also, one can observe that the level of pressure decreases as We increases (see the section zoomed). In addition, a sharp linear decline in pressure through the rest of the channel occurs, reaching zero at the outer-conduit. For more detail, pressure drop is plotted as a function of We in Figure 5(b). These results are consistent with the findings of others [18,21].

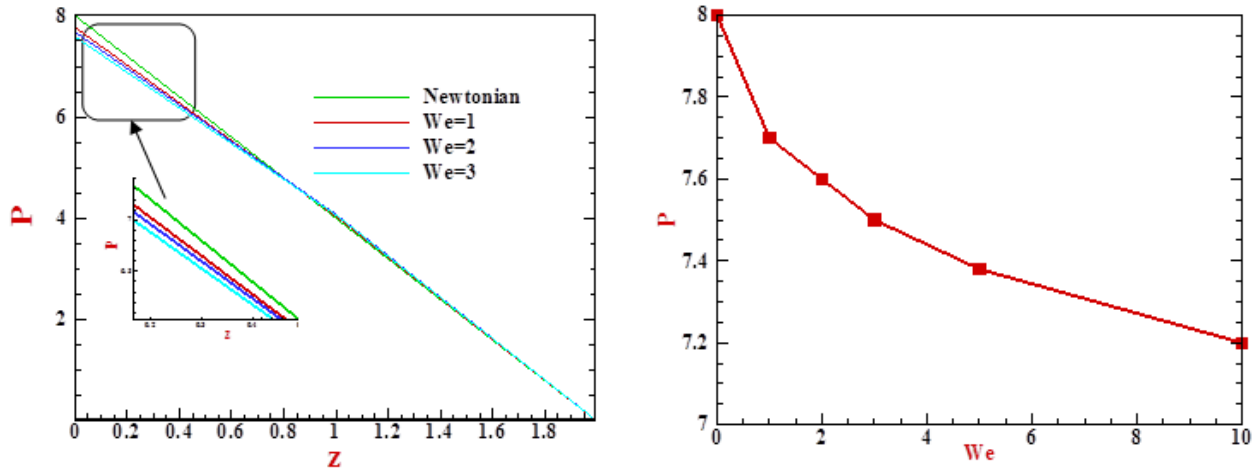

(a) (b)

Fig. 5. (a) Pressure drop profiles on axis of symmetry (b) Pressure as a function of We, $\beta = 0.9$

For $We = \{1,2,3\}$ setting and $\beta = 0.9$, the shear stress τ_{rz} and normal stress τ_{zz} along top surface are provided in Figure 6. The results show that, for τ_{rz} one can observed that the change in the level of τ_{rz} is occurred at the outlet of the channel, such that this level is raised as We increases (see Figure 6(a)). Once more, the influence of shear-thinning would dominate the levels of τ_{zz}, where the high level is appeared at outlet of the channel. From the profiles we can see that the maximum level of τ_{rz} is observed at the inlet of the channel for all We-values, reaching around -0.002 unit, while the maximum τ_{zz} is occurred at the largest We: at $We = 3$ normal stress reaches levels of around 0.9 unit (see Figure 6(b)).

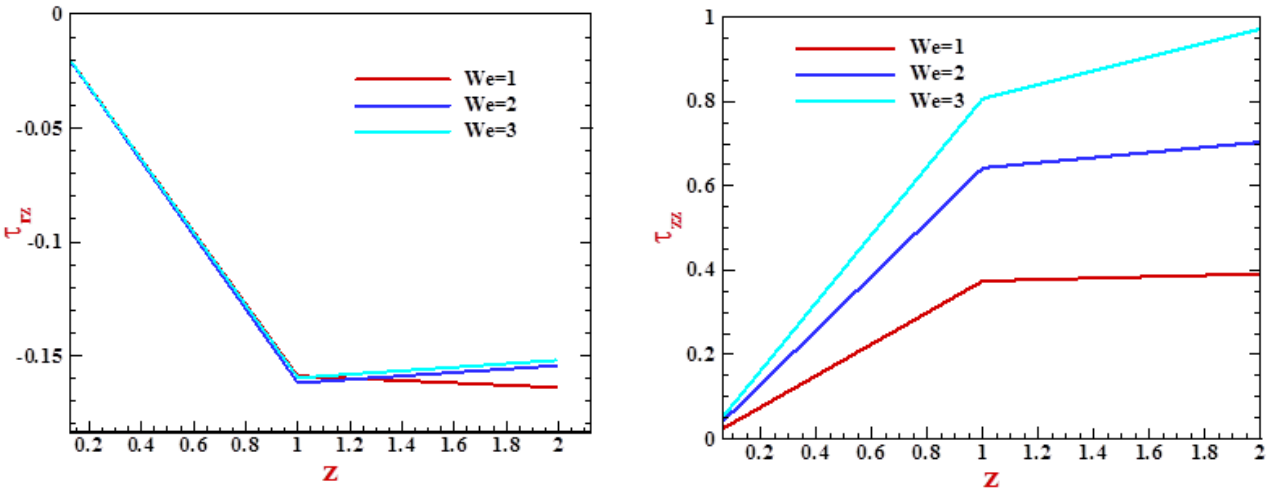

(a) (b)

Fig. 6. Stress profiles along top surface; We-variation, $\beta = 0.9$, (a) shear stress τ_{rz} (b) normal stress τ_{zz}

Extensional data of the maximum and minimum values of all solutions components are presented in Table 2. Here, the radial velocities show little change for each We, while an increasing in pressure maxima is displayed with rising We. In all cases of stress components and increasing We-value, there is slight raise.

Table 2
Velocity, pressure and Stresses; We-variation, $\beta = 0.9$

We	u_z	p	τ_{rz}	τ_{zz}	τ_{rr}
1	$Max = 1.014$ $Min = 0$	$Max = 7.799$ $Min = 0$	$Max = 0$ $Min = -0.164$	$Max = 0.391$ $Min = 0$	$Max = 0.0001$ $Min = 0$
2	$Max = 1.087$ $Min = 0$	$Max = 7.678$ $Min = 0$	$Max = 0$ $Min = -0.619$	$Max = 0.704$ $Min = 0$	$Max = 0.0002$ $Min = 0$
3	$Max = 1.0217$ $Min = 0$	$Max = 7.584$ $Min = 0$	$Max = 0$ $Min = 0.596$	$Max = 0.972$ $Min = 0$	$Max = 0.0003$ $Min = 0$

Moreover, Figure 7 displays the rate of convergence for pressure ($HSTP$), velocity ($HSTV$) and stress ($HISTS$) under two different β-values ($\beta = \{1/9, 0.9\}$) and $We = 1$. Generally, for both β-values the same temporal convergence trends occur in pressure (also in velocity). Under the highest solvent fraction ($\beta = 0.9$), the prediction error was less than with another solvent fraction ($\beta = 1/9$) to reach the tolerance level. For the stress, one can observe that for the larger time-steps the discretisation error is minimal under $\beta = 1/9$ to attain the convergence criteria (see Figure 7(c)).

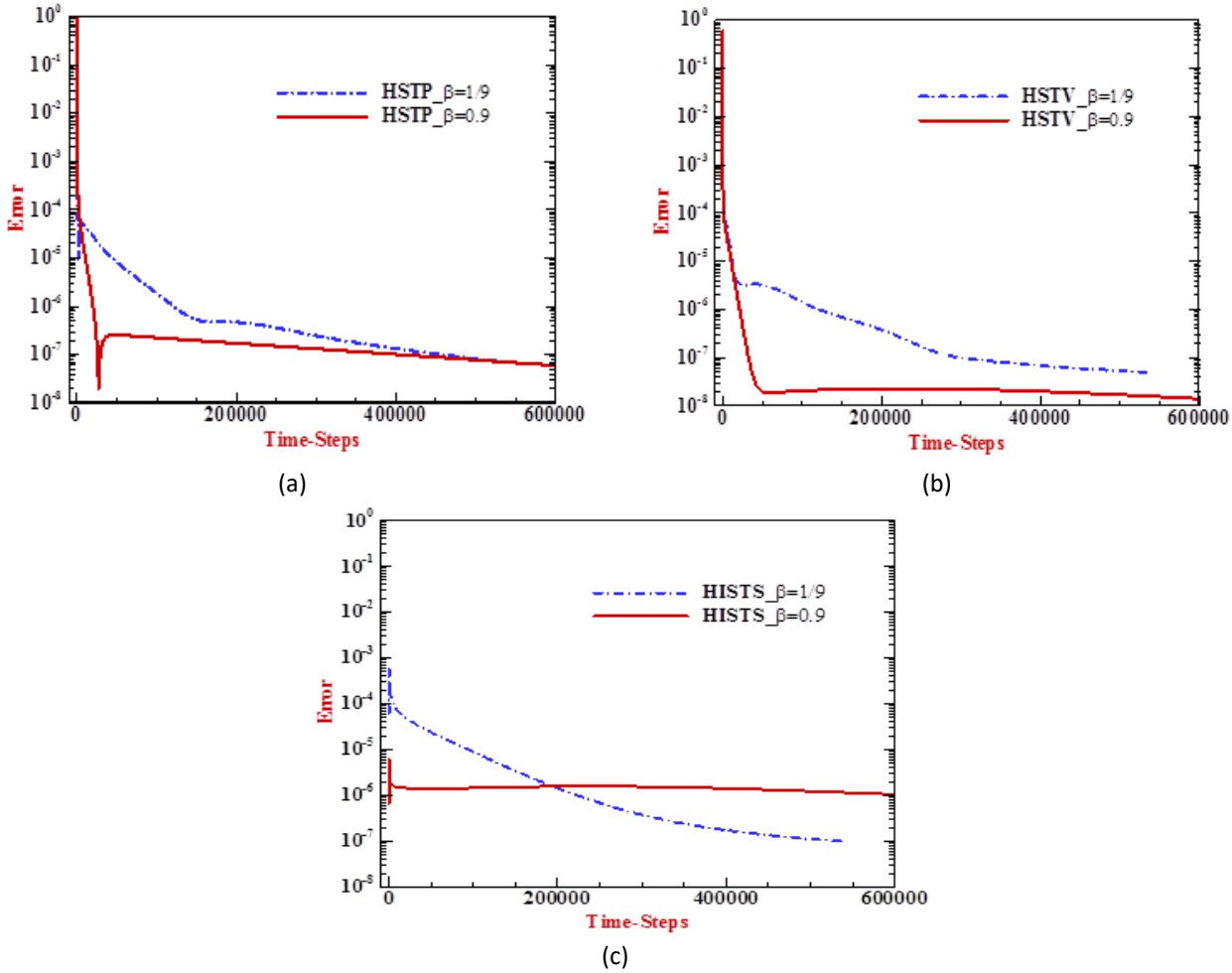

Fig. 7. Rate of convergence, (a) Pressure, (b) Velocity, (c) Stress; $We = 1$, $\beta = 0.9, 1/9$

In contrast to the foregoing, we next consider the influence of solvent fraction (β) through the variation in We. Table 3 provides the maximum level of all solution for two different β-values ($\beta = \{0.9, 1/9, 0.05\}$) and $We = \{1,2,3\}$. The findings reveal that there is a modest increase in the velocity maxima, where recorded the slightly high level with $\beta = 1/9$. On the other hand, one can observe a

significant alteration in the normal stress maxima in the case of $\beta = 1/9$ compared to that with $\beta = 0.9$. In this situation, it is notable that the normal and radial stresses strongly raise with $\beta = 1/9$. For example, at $We = 3$ the peak level of τ_{zz} is 0.961 units with $\beta = 0.9$, but it is around 11.855 units and 12.628 units for $\beta = 1/9$ and $\beta = 0.05$, respectively. For the pressure the trend oppose those observed for stress, in that a decrease is occurred in the p maxima for $\beta = 1/9$.

Table 3
Maximum value: velocity, pressure and stresses; We-variation, β-variation

Maximum value	$\beta = 0.9$				$\beta = 1/9$			$\beta = 0.05$	
	$We = 1$	$We = 2$	$We = 3$	$We = 1$	$We = 2$	$We = 3$	$We = 1$	$We = 2$	$We = 3$
u_z	1.0149	1.0187	1.0216	1.39	1.686	1.787	1.78	2.76	3
p	7.798	7.679	7.584	6.667	6.497	6.207	6.415	6.358	6.132
τ_{rr}	0.0005	0.0009	0.0006	0.318	0.111	0.086	0.504	0.66	0.096
τ_{zz}	0.39	0.697	0.961	13.191	12.232	11.855	14.428	14.13	12.628
$\tau_{\theta\theta}$	0.0037	0.0053	0.0057	2.471	2.106	1.985	2.5	2.983	3.104

The shear stress (τ_{rz}), normal stress (τ_{zz}), radial stress and azimuthal stress profiles are illustrated in Figure 8 through increasing We and fixed $\beta = 1/9$ along the top wall. Generally, the findings display a reducing trend in peak values as We increases in stress components, which is consistent with results reported by other researchers [16,33].

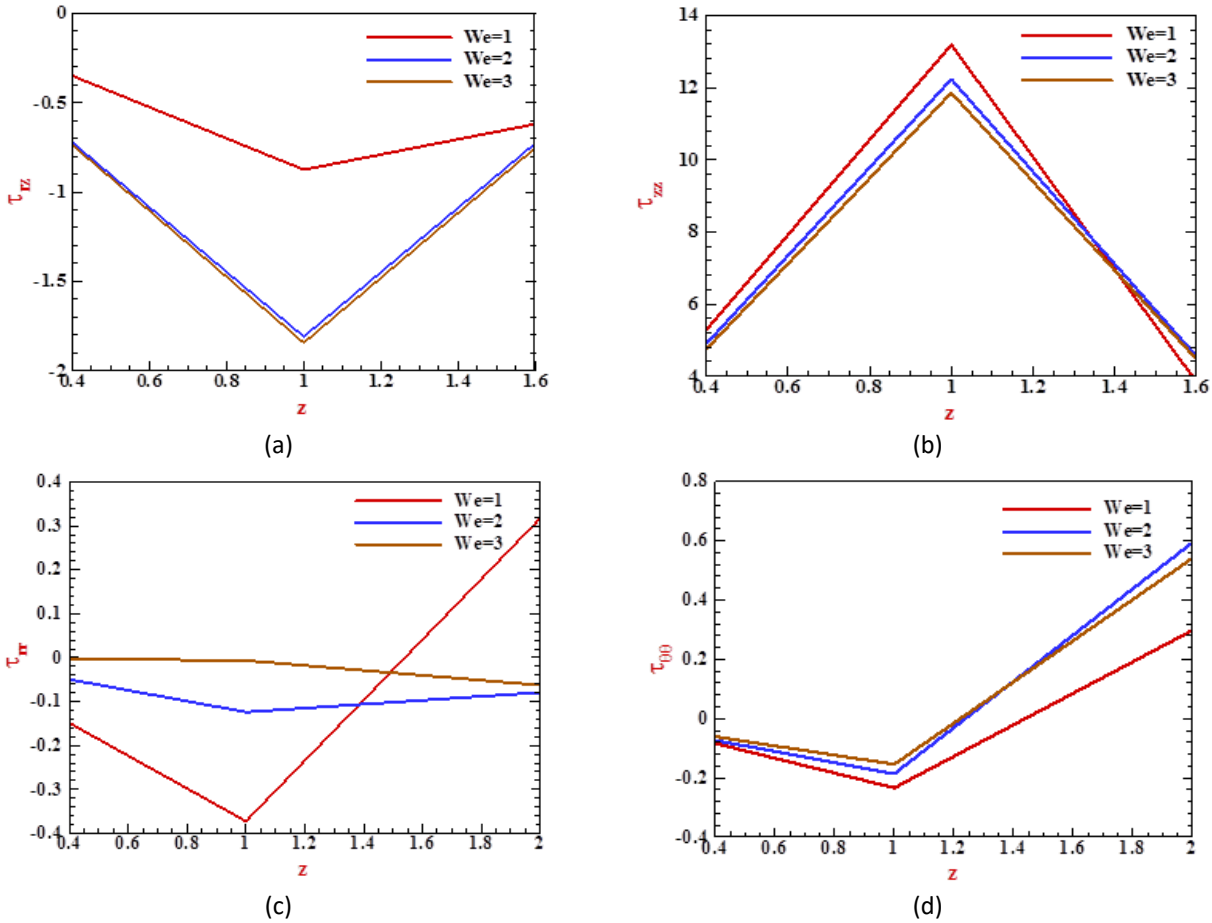

Fig. 8. Stress profiles along top surface; We-variation, $\beta = 1/9$ (a) τ_{rz}(b) τ_{zz} (c) τ_{rr} (d) $\tau_{\theta\theta}$

5.1 Pressure Coefficient (C_p)

Other finding of our investigation is the pressure coefficient (C_p), which is defined as

$$C_p = \frac{p_1 - p_0}{\frac{1}{2}\rho \overline{U}^2}. \tag{27}$$

where, p_1 is the pressure at the channel inlet, p_0 is the pressure at the channel outlet, ρ is the density, and $\overline{U}$ is the average velocity. Here, the pressure coefficient is studied for different setting of We and solvent-fraction with Reynolds number of unity. Consequently, Figure 9 illustrates the C_p as a function of We with $\beta = \{0.9, 1/9, 0.05\}$. Overall, the plot exhibits a major difference in C_p with variation in solvent-fractionβ. The highest value for $C_p$is observed with high solvent fraction ($\beta = 0.9$), due to dominant shear-thinning influence. In contrast, the data reveal that, the C_p level decreases as We increases. For instance, with $We = 1$ the maximum level of C_p for $\beta = 0.9$ is around 60 units, compared to 27 units for $\beta = 1/9$ and 16 unit for $\beta = 0.05$; almost $O(55\%)$ and $O(73\%)$ reduction, respectively.

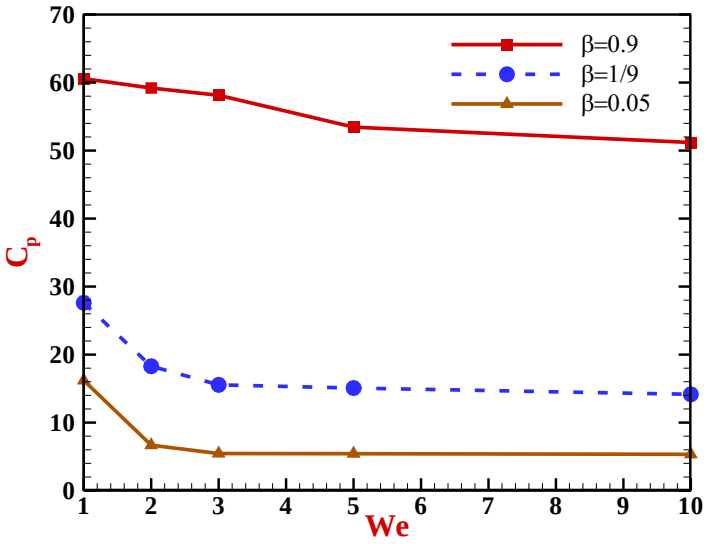

Fig. 9. Pressure drop coefficient for $Re = 1$, We-variation and β-variation

6. Conclusions

In this paper, the numerical solutions for Oldroyd-B viscoelastic fluid in axisymmetric straight channel by using a hybrid finite element/volume method $fe/fv(sc)$ in cylindrical coordinates system are presented. High accuracy has been shown by comparing the numerical results with analytic solutions for the velocity and stress under specific conditions. The rate of convergence of the solution components under $fe/fv(sc)$ method is provided in this study. With the selected set of parameters, we have commenced with a Weissenberg number (We) and solvent fraction (β). The respective influences of velocity, pressure and stresses with We-variation and use three different values of solvent fraction $\beta = \{0.9, 1/9, 0.05\}$ have been systematically investigated. The results show that, less time is required in velocity development compared to pressure and stress development. The pressure drop with We-variation is introduced, such that there is no significant change observed except in the inlet of the channel. On the maxima level of solution components for $\beta =$

$\{0.9, 1/9, 0.05\}$ and We-variation it is notable that radial and normal stresses strongly amplify, while no significant change is observed for remaining components.

References

[1] Wapperom, P., and M. F. Webster. "A second-order hybrid finite-element/volume method for viscoelastic flows." *Journal of Non-Newtonian Fluid Mechanics* 79, no. 2-3 (1998): 405-431. https://doi.org/10.1016/S0377-0257(98)00124-4

[2] Struijs, R., Herman Deconinck, and P. L. Roe. "Fluctuation splitting schemes for the 2D Euler equations." In its *Computational Fluid Dynamics 94 p (SEE N91-32426 24-34* (1991).

[3] Carew, E. O. A., P. Townsend, and M. F. Webster. "A Taylor-Petrov-Galerkin algorithm for viscoelastic flow." *Journal of Non-Newtonian Fluid Mechanics* 50, no. 2-3 (1993): 253-287. https://doi.org/10.1016/0377-0257(93)80034-9

[4] Baloch, A., P. Townsend, and M. F. Webster. "On the simulation of highly elastic complex flows." *Journal of Non-Newtonian Fluid Mechanics* 59, no. 2-3 (1995): 111-128. https://doi.org/10.1016/0377-0257(95)01369-7

[5] Baloch, A., P. Townsend, and M. F. Webster. "On vortex development in viscoelastic expansion and contraction flows." *Journal of Non-Newtonian Fluid Mechanics* 65, no. 2-3 (1996): 133-149. https://doi.org/10.1016/0377-0257(96)01470-X

[6] Xue, S-C., N. Phan-Thien, and R. I. Tanner. "Three dimensional numerical simulations of viscoelastic flows through planar contractions." *Journal of Non-Newtonian Fluid Mechanics* 74, no. 1-3 (1998): 195-245. https://doi.org/10.1016/S0377-0257(97)00072-4

[7] Baaijens, Frank PT. "Numerical analysis of unsteady viscoelastic flow." *Computer Methods in Applied Mechanics and Engineering* 94, no. 2 (1992): 285-299. https://doi.org/10.1016/0045-7825(92)90151-9

[8] Béraudo, C., A. Fortin, T. Coupez, Y. Demay, B. Vergnes, and J. F. Agassant. "A finite element method for computing the flow of multi-mode viscoelastic fluids: comparison with experiments." *Journal of Non-Newtonian Fluid Mechanics* 75, no. 1 (1998): 1-23. https://doi.org/10.1016/S0377-0257(97)00083-9

[9] Hirsch, Charles. *Numerical computation of internal and external flows, Volume 1. Fundamentals of numerical discretization*. John Wiley and Sons 9, 1988.

[10] Sato, Toru, and Stephen M. Richardson. "Explicit numerical simulation of time-dependent viscoelastic flow problems by a finite element/finite volume method." *Journal of Non-Newtonian Fluid Mechanics* 51, no. 3 (1994): 249-275. https://doi.org/10.1016/0377-0257(94)85019-4

[11] Yoo, Jung Yul, and Yang Na. "A numerical study of the planar contraction flow of a viscoelastic fluid using the SIMPLER algorithm." *Journal of Non-Newtonian Fluid Mechanics* 39, no. 1 (1991): 89-106. https://doi.org/10.1016/0377-0257(91)80005-5

[12] Wapperom, P., and M. F. Webster. "Simulation for viscoelastic flow by a finite volume/element method." *Computer Methods in Applied Mechanics and Engineering* 180, no. 3-4 (1999): 281-304. https://doi.org/10.1016/S0045-7825(99)00170-X

[13] Aboubacar, M., and M. F. Webster. "A cell-vertex finite volume/element method on triangles for abrupt contraction viscoelastic flows." *Journal of Non-Newtonian Fluid Mechanics* 98, no. 2-3 (2001): 83-106. https://doi.org/10.1016/S0377-0257(00)00196-8

[14] Aboubacar, M., H. Matallah, and M. F. Webster. "Highly elastic solutions for Oldroyd-B and Phan-Thien/Tanner fluids with a finite volume/element method: planar contraction flows." *Journal of Non-Newtonian Fluid Mechanics* 103, no. 1 (2002): 65-103. https://doi.org/10.1016/S0377-0257(01)00164-1

[15] Webster, M. F., H. R. Tamaddon-Jahromi, and M. Aboubacar. "Time-dependent algorithms for viscoelastic flow: Finite element/volume schemes." *Numerical Methods for Partial Differential Equations: An International Journal* 21, no. 2 (2005): 272-296. https://doi.org/10.1002/num.20037

[16] Belblidia, Fawzi, I. J. Keshtiban, and M. F. Webster. "Stabilised computations for viscoelastic flows under compressible implementations." *Journal of Non-Newtonian Fluid Mechanics* 134, no. 1-3 (2006): 56-76. https://doi.org/10.1016/j.jnnfm.2005.12.003

[17] Belblidia, F., H. Matallah, B. Puangkird, and M. F. Webster. "Alternative subcell discretisations for viscoelastic flow: Stress interpolation." *Journal of Non-Newtonian Fluid Mechanics* 146, no. 1-3 (2007): 59-78. https://doi.org/10.1016/j.jnnfm.2006.12.009

[18] Al-Muslimawi, Alaa Hasan A. *Numerical analysis of partial differential equations for viscoelastic and free surface flows*. Swansea University (United Kingdom), 2013.

[19] Al-Muslimawi, A., H. R. Tamaddon-Jahromi, and M. F. Webster. "Numerical simulation of tube-tooling cable-coating with polymer melts." *Korea-Australia Rheology Journal* 25, no. 4 (2013): 197-216. https://doi.org/10.1007/s13367-013-0021-x

[20] Al-Muslimawi, A., H. R. Tamaddon-Jahromi, and M. F. Webster. "Numerical computation of extrusion and draw-extrusion cable-coating flows with polymer melts." *Applied Rheology* 24, no. 3 (2014): 1-15.
[21] Al-Muslimawi, Alaa H. "Numerical study for differential constitutive equations with polymer melts by using a hybrid finite-element/volume method." *Journal of Computational and Applied Mathematics* 308 (2016): 488-498. https://doi.org/10.1016/j.cam.2016.06.007
[22] Sulochana, Chalavadi, Samrat S. Payad, and Naramgari Sandeep. "Non-uniform heat source or sink effect on the flow of 3D Casson fluid in the presence of Soret and thermal radiation." In *International Journal of Engineering Research in Africa*, vol. 20, pp. 112-129. Trans Tech Publications Ltd, 2016. https://doi.org/10.4028/www.scientific.net/JERA.20.112
[23] Sulochana, C., S. P. Samrat, and N. Sandeep. "Numerical investigation of magnetohydrodynamic (MHD) radiative flow over a rotating cone in the presence of Soret and chemical reaction." *Propulsion and power Research* 7, no. 1 (2018): 91-101. https://doi.org/10.1016/j.jppr.2018.01.001
[24] Tlili, Iskander, S. P. Samrat, N. Sandeep, and Hossam A. Nabwey. "Effect of nanoparticle shape on unsteady liquid film flow of MHD Oldroyd-B ferrofluid." *Ain Shams Engineering Journal* (2020). https://doi.org/10.1016/j.asej.2020.06.007
[25] Samrat, S. P., C. Sulochana, and G. P. Ashwinkumar. "Impact of thermal radiation on an unsteady Casson nanofluid flow over a stretching surface." *International Journal of Applied and Computational Mathematics* 5, no. 2 (2019): 1-20. https://doi.org/10.1007/s40819-019-0606-2
[26] Tlili, Iskander, Hossam A. Nabwey, S. P. Samrat, and N. Sandeep. "3D MHD nonlinear radiative flow of CuO-MgO/methanol hybrid nanofluid beyond an irregular dimension surface with slip effect." *Scientific Reports* 10, no. 1 (2020): 1-14. https://doi.org/10.1038/s41598-020-66102-w
[27] Townsend, P., and M. F. Webster. "An algorithm for the three-dimensional transient simulation of non-Newtonian fluid flows." In *Proc. Int. Conf. Num. Meth. Eng.: Theory and Applications, NUMETA, Nijhoff, Dordrecht*, vol. 12, pp. 1-11. 1987.
[28] Zienkiewicz, O. C., K. Morgan, J. Peraire, M. Vandati, and R. Löhner. "Finite elements for compressible gas flow and similar systems." In *7th Int. Conf. Comput. Meth. Appl. Sci. Eng.* 1985.
[29] Donea, J. "A Taylor-Galerkin algorithm for hyperbolic conservation laws." *International Journal for Numerical Methods in Engineering* 20 (1984): 101-119. https://doi.org/10.1002/nme.1620200108
[30] Matallah, H., P. Townsend, and M. F. Webster. "Recovery and stress-splitting schemes for viscoelastic flows." *Journal of Non-Newtonian Fluid Mechanics* 75, no. 2-3 (1998): 139-166. https://doi.org/10.1016/S0377-0257(97)00085-2
[31] Aboubacar, M., H. Matallah, H. R. Tamaddon-Jahromi, and M. F. Webster. "Numerical prediction of extensional flows in contraction geometries: hybrid finite volume/element method." *Journal of Non-Newtonian Fluid Mechanics* 104, no. 2-3 (2002): 125-164. https://doi.org/10.1016/S0377-0257(02)00015-0
[32] Bird, R. Byron, Warren E. Stewart, Edwin N. Lightfoot, and Daniel J. Klingenberg. *Introductory Transport Phenomena*. Wiley, 2014.
[33] Ngamaramvaranggul, V., and M. F. Webster. "Viscoelastic simulations of stick-slip and die-swell flows." *International Journal for Numerical Methods in Fluids* 36, no. 5 (2001): 539-595. https://doi.org/10.1002/fld.145